Proceedings of the ASME 2018 37th International Conference on Ocean, Offshore and Arctic Engineering
OMAE2018
June 17-22, 2018, Madrid, Spain

OMAE2018-78373

NUMERICAL INVESTIGATION OF REGULAR WAVES INTERACTION WITH TWO FIXED CYLINDERS IN TANDEM ARRANGEMENT

Zhenghao Liu
Collaborative Innovation Center for Advanced Ship and Deep-Sea Exploration, State Key Laboratory of Ocean Engineering, School of Naval Architecture, Ocean and Civil Engineering, Shanghai Jiao Tong University, Shanghai 200240, China

Decheng Wan*
Collaborative Innovation Center for Advanced Ship and Deep-Sea Exploration, State Key Laboratory of Ocean Engineering, School of Naval Architecture, Ocean and Civil Engineering, Shanghai Jiao Tong University, Shanghai 200240, China
*Corresponding author:
dcwan@sjtu.edu.cn

Changhong Hu
Research Institute for Applied Mechanics,
Kyushu University,
Fukuoka, Kasuga,
Japan 816-8580

ABSTRACT

The interaction of waves with fixed or floating structures involves complex wave radiation, wave diffraction and free surface deformation. In this work, the interaction of waves with a pair of cylinders in tandem arrangement is investigated using a numerical wave tank. The numerical simulation is first validated by comparing numerical results and experimental data for regular wave interaction with a single cylinder. Wave interaction with tandem cylinders is investigated for different center-to-center distances between the cylinders.

All the numerical simulations are carried out by the in-house CFD solver naoe-FOAM-SJTU which is developed on the open source platform OpenFOAM. The incompressible unsteady Reynolds averaged Navier-Stokes (URANS) equations are adopted as the governing equations. The volume of fluid (VOF) method is applied to capture the free surface. The surface elevation around the cylinders is probed by a series of wave gauges and analyzed using transfer function. The wave forces of upstream and downstream cylinder are discussed in detail. The wave forces experienced by the tandem cylinders is highly influenced by the distance between the cylinders. The local surface elevation and the scattered wave field around the cylinders are also investigated. The results show that the present CFD solver can be an alternative tool to deal with wave-structure interactions.

INTRODUCTION

Cylindrical columns are commonly used as support structures of offshore platforms, which are widely applied in ocean engineering. As we know, wave-structure interaction involves in complex wave radiation and wave diffraction, especially for large-scale structures. In some severe environment, wave run-up on the cylinders of the structures can be relatively large and even causes green water on deck. To predict the hydrodynamics loads on these structures accurately, it is important to understand the nonlinear wave-structure interaction. For a circular cylinder, the contribution of drag and inertia forces to the total forces is generally determined by the Keulegan-Carpenter number (KC=$\boldsymbol{U}T/D$, where $\boldsymbol{U}$ is the wave-induced velocity amplitude, T is the wave period and D is the diameter of the cylinder) and the diffraction parameter. If the KC number is smaller than 2 and the diffraction parameter (D/L, where L is the incident wavelength) is greater than 0.2, the flow is inertia dominated and wave diffraction effects are important.

Numerous researchers have done lots of studies on wave interaction with single fixed cylinder. Galvin and Hallermeier [1] experimentally studied the distribution of free surface around a circular cylinder by mounting a series of wave gauges near the column. It was found that the wave run-up can be affected by scattering effect and viscous dissipation effect. Both Chakrabarti and Tam [2] and Morris-Thomas et al. [3] investigated the scattering effect and viscous dissipation effect

by conducting several model tests of regular waves onto a large-scale cylinder. Theoretical methods based on Morison equation or potential flow theory have also been used to study wave-structure interaction. The approximate results of wave run-up on a single cylinder were acquired according to first- and second-order potential flow theory [4-5] and fully nonlinear numerical wave tanks (NWT) [6-8]. Trulsen and Teigen [6] found the effects of viscosity may take account for the discrepancies between the theoretical method and experiment. Recently, computational fluid dynamics (CFD) method based on Navier-Stokes equations has been widely applied in ocean engineering field. Based on the open source platform OpenFOAM, Cao and Wan [9-11] simulated the regular and solitary waves on to a circular cylinder, and the predicted results of wave run-up showed the reasonable agreement with experimental data. Sun et al. [12] used a both potential flow solver DIFFRACT and a full CFD solver OpenFOAM to investigate nonlinear interactions between regular waves and a single truncated circular column. The predicted free surface elevation around the column and the wave forces were analyzed and compared with experimental data. The ITTC committee organized experimental and numerical researches for the investigations of wave run-up on a single cylinder and four cylinders in square arrangement [13]. The provided experimental data are adopted as validation of the numerical simulation in this work.

Most platforms in offshore engineering are supported by multi-column structures. Thus, investigation of wave interaction with multiple cylinders is of great importance. Many researchers have been focused on wave interaction with multi-column platforms or an array of cylinders. Niedzwecki and Huston [14] experimentally studied the wave run-up on a TLP in regular waves. Contento et al. [15] studied the wave interaction with an array of vertical cylinders and found the second-order crest near cylinder shoulder. Ma et al. [16] investigated the full nonlinear diffraction around a pair of vertical cylinders based on finite element method. Stansberg and Kristiansen [17] studied the nonlinear wave-column interaction in steep waves with second-order numerical model. Ohl et al. [18-19] studied regular and irregular wave interaction with an array of cylinders, and good agreement between the theory and the laboratory results was found. Based on the linear theory of wave interaction with an array of circular bottom-mounted vertical cylinders, Ji et al. [20] investigated the effects of the wave directionality on wave loads in real conditions. It was found that the wave directionality has a significant influence on the transverse force. Kamath et al. [21] used CFD model to investigate the wave forces and the flow field around cylinders placed in a regular wave field. The wave interaction with a single large cylinder and a pair of large cylinders placed in tandem for different incident wave steepnesses and different center-to-center distances was studied. Zhong and Yeung [22] developed a semi-analytical method to investigate wave radiation and diffraction by an array of truncated vertical cylinders and compared hydrodynamic coefficients and wave-exciting loads with other methods.

The objective of the present work is to investigate the regular wave interaction with two tandem cylinders for different center-to-center distances. The computations in this paper are performed with the in-house CFD solver naoe-FOAM-SJTU. The numerical results of the RAO around single cylinder are presented and compared with experiments performed at MOERI [13]. The wave forces of two cylinders in tandem arrangement are discussed in detail. The local surface elevation and the scattered wave field around the cylinders are also investigated. The results show that the present approach can be an alternative tool to deal with nonlinear wave-structure interactions.

NUMERICAL METHODS

Governing equations

The CFD solver naoe-FOAM-SJTU is based on the open source platform OpenFOAM and designed for the application in ship and ocean engineering field [23-27]. Compared to the OpenFOAM standard solver, the naoe-FOAM-SJTU solver is complemented with a wave generation and damping module, a wave probe module, a 6DoF motion module, a mooring system module and turbulence models and can be used to simulate wave-structure interaction.

The naoe-FOAM-SJTU solver uses the incompressible unsteady Reynolds averaged Navier-Stokes (URANS) equations with the continuity equation to solve the fluid flow problem:

$$\nabla \cdot \boldsymbol{U} = 0 \tag{1}$$

$$\frac{\partial \rho \boldsymbol{U}}{\partial t} + \nabla \cdot (\rho(\boldsymbol{U} - \boldsymbol{U}_g)\boldsymbol{U}) = -\nabla p_d - \boldsymbol{g} \cdot x \nabla \rho + \nabla \cdot (\mu_{eff} \nabla \boldsymbol{U}) + (\nabla \boldsymbol{U}) \cdot \nabla \mu_{eff} + f_\sigma + f_s \tag{2}$$

where $\boldsymbol{U}$ and $\boldsymbol{U_g}$ are the velocity field and the velocity of grid nodes, respectively. p_d is the dynamic pressure and p is the total pressure, ρ is the mixed density of the two phases water and air. μ_{eff} is the effective dynamic viscosity, in which ν and ν_t are kinematic viscosity and eddy viscosity, respectively. f_σ is the surface tension, which impacts the free surface. f_s is a source term, added to generate the sponge layer for wave absorbing.

Free surface

Volume of fluid (VOF) method [28] with artificial bounded compression techniques is adopted in naoe-FOAM-SJTU solver to capture the free surface of the two-phase flow. The method is based on a volume fraction α which can control numerical diffusion and capture the interface with high resolution. The volume fraction function can be determined by solving a transport equation:

$$\frac{\partial \alpha}{\partial t} + \nabla \cdot [(\boldsymbol{U} - \boldsymbol{U}_g)\alpha] + \nabla \cdot [\boldsymbol{U}_r (1-\alpha)\alpha] = 0 \tag{3}$$

The first two terms on the left-hand side of Eq. (3) stand for traditional volume of fluid transport equation while the third term represents the artificial compression term. The compression velocity $\boldsymbol{U_r}$ [Weller *et al*. (1998)] is computed at

cell faces by the maximum velocity magnitude at the interface region:

$$U_{r,f} = n_f \min\left\{C_\alpha \frac{|\phi|}{|S_f|}, \max\left(\frac{|\phi|}{|S_f|}\right)\right\} \quad (4)$$

where φ is face volume flux; C_α is a compression coefficient controlling the magnitude of compression, in this paper it is chosen to be 1.0. Larger value will increase the compression of the interface, leading to larger detrimental velocity gradients around the interface. The compression term only works on the interface without affecting the numerical computation out of the transition layer due to term $(1-\alpha)\alpha$.

Different phases are marked using volume fraction α which indicates the relative proportion of fluid in each cell, it is defined as Eq. (5). For an interface cell, the value of volume fraction α is between 0 and 1, representing it contains both water and air.

$$\begin{cases} \alpha=0 & \text{air} \\ \alpha=1 & \text{water} \\ 0<\alpha<1 & \text{interface} \end{cases} \quad (5)$$

In physical domain, the density of fluid ρ and the dynamic viscosity μ can be obtained by a weighted value based on the volume fraction α:

$$\rho = \alpha\rho_1 + (1-\alpha)\rho_2 \quad (6)$$

$$\mu = \alpha\mu_1 + (1-\alpha)\mu_2 \quad (7)$$

Where ρ_1 and $\rho_2$denote the density of water and air, μ_1 and μ_2 denote the viscosity coefficient of water and air, respectively.

Numerical wave tank

A wave generation and damping module are extended to the in-house naoe-FOAM-SJTU solver. Generally, the velocity inlet is adopted to generate regular or irregular waves. To generate the Stokes first deep-water wave, the inlet boundary conditions are set as follows:

$$\eta = a\cos(\mathbf{k}\cdot\mathbf{x} - \omega_e t + \delta) \quad (8)$$

$$u = U_0 + a\omega e^{kz}\cos(\mathbf{k}\cdot\mathbf{x} - \omega t + \delta) \quad (9)$$

$$v = a\omega e^{kz}\cos\beta\cos(\mathbf{k}\cdot\mathbf{x} - \omega t + \delta) \quad (10)$$

$$w = a\omega e^{kz}\sin\beta\sin(\mathbf{k}\cdot\mathbf{x} - \omega t + \delta) \quad (11)$$

Where ζ is transient wave elevation, a, ω and $\boldsymbol{k}$ are wave amplitude, wave frequency and wave number, respectively. $\boldsymbol{U_0}$ is hull speed, β represents wave incident direction.

To avoid wave reflection, a sponge layer is setup at the outlet of the computational domain. The term of f_s is introduced into Eq. (2) for absorption of waves and defined as:

$$f_s(x) = \begin{cases} -\rho\alpha_s\left(\frac{x-x_s}{L_s}\right)^2(U-U_{ref}) \\ 0 \end{cases} \quad (12)$$

Where ρ is the water density. The α_s is an artificial viscosity coefficient controlling the intensity of the sponge layer. The x_s is the coordinate of the start position of the sponge layer and L_s is the length of the sponge layer. The source term f_s has no effects on the domain out of the sponge layer.

Discretization schemes

The finite volume method (FVM) is adopted to discretize the RANS and VOF transport equations in OpenFOAM. Van Leer scheme is applied for VOF equation. The PIMPLE (merged PISO-SIMPLE) algorithm is used to solve the coupled equation of velocity and pressure. The convection terms are solved by a second-order TVD limited linear scheme, and the diffusion terms are approximated by a second-order central difference scheme.

NUMERICAL SIMULATION

Grid convergence study of wave generation

Accurate wave generation is of great importance in the numerical simulation. Generally, the magnitude of discretization error in numerical simulation can be verified by grid convergence study. A numerical wave tank with a length of 5L, width of 2L and height of 1.5L is used in this work, where L is the wavelength of 76.44 m. Grid convergence examinations are performed for the Stokes first-order waves of T = 7s and H/L =1/30 without cylinder. According to the experiments, the errors arising from extrapolation can be reduced if the refinement ratio of r > 1.3 [29]. In this study, a refinement ratio of $r = \sqrt{2}$ in each direction is selected. The total number of coarse mesh (mesh1), medium mesh (mesh2) and fine mesh (mesh3) are 0.33M, 0.96M and 2.71M, respectively. Stern et al. [30] proposed a verification method to estimating uncertainty due to grid and time step errors. The convergence solution (R_G) of different solutions (S_i) is defined as:

$$R_G = \frac{S_2 - S_1}{S_3 - S_2} \quad (13)$$

where S_i corresponds to solutions with fine, medium and coarse grid, respectively. And different R_G values represent different convergence conditions: (1) $0 < R_G < 1$ represents monotonic convergence, and generalized Richardson extrapolation (RE) is used to estimate grid uncertainty. (2) $R_G < 0$ represents oscillatory convergence, and uncertainties can be estimated by attempting to bound the error based on oscillation maximums S_U and minimums S_L. (3) $R_G > 1$ represents divergence, and uncertainties cannot be estimated. Fig. 1 shows the time histories of surface elevations without cylinder at different locations for the three meshes. The results show good convergence at x=0 and 8 m. As the grid is refined, the total wave amplitude approaches the theoretical data monotonically. The medium mesh is used as background mesh for the remaining simulations.

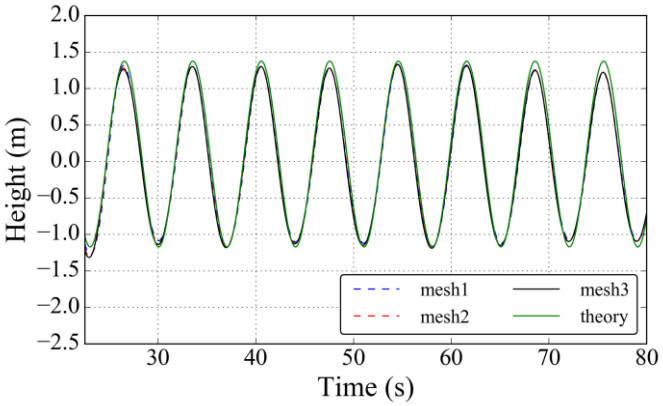

x=-16 m

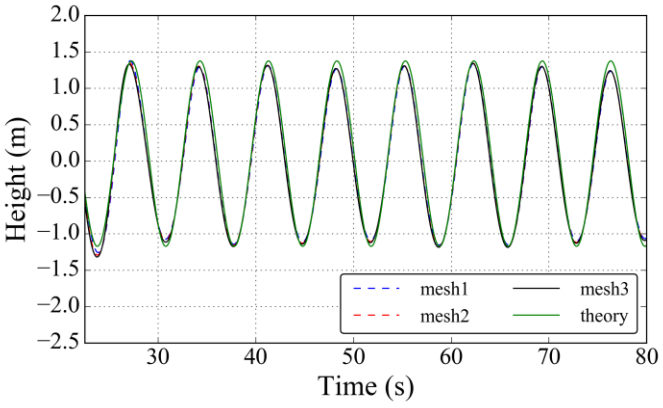

x=-8 m

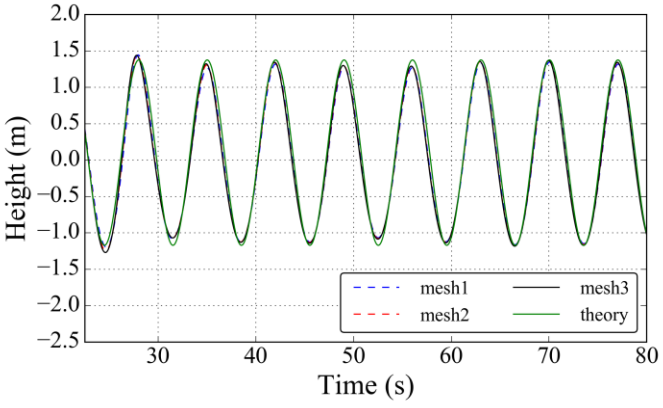

x=0 m

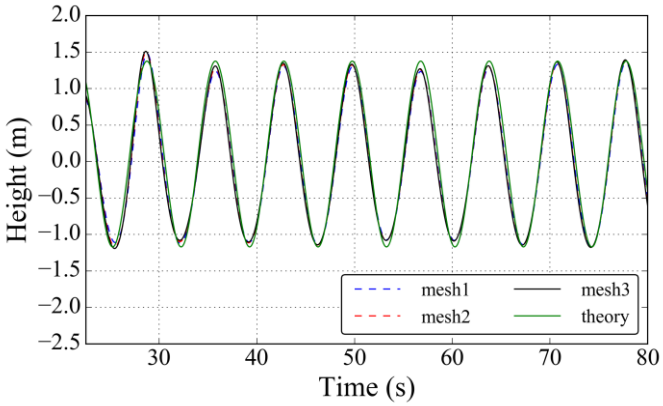

x=8 m

Fig. 1. Time histories of surface elevations without cylinder based on different meshes

Wave interaction with a single large cylinder

To simulate wave run-up on a truncated surface-piercing column, the cylinder model at full scale from MOERI is selected in numerical simulation. The radius of the cylinder is R = 8.0 m, and the draft is 24.0 m. A series of wave probes in both experiment and numerical simulation are shown in Fig. 2, and the corresponding location are given in Table 1. The distances to the cylinder for inner circle wave probes and outer circle wave probes are 0.2063 m and 8 m, respectively.

The Stokes first-order deep water wave is applied in the present work. One wave period (T = 7s) and three steepness parameters (H/L = 1/30, 1/16 and 1/10) were simulated, where H is the wave height and L is the wavelength.

The numerical wave tank extends to $-2L < x < 3L$, $-L < y < L$, $-L < z < 0.5L$, as shown in Fig. 3. The water depth is set as one wavelength L. The length of sponge length is also set as L, starting from $x = 2L$. About 70 grids per wavelength and 20 per wave height are applied in the present work. The total grid number is about 1.7 million. The time step is 0.005s in each case. The cylinder is set as rigid walls with no-slip boundary conditions. No wall function is applied in this study. Turbulence modeling is carried out using laminar flow, as suggested by Sun et al. [12]

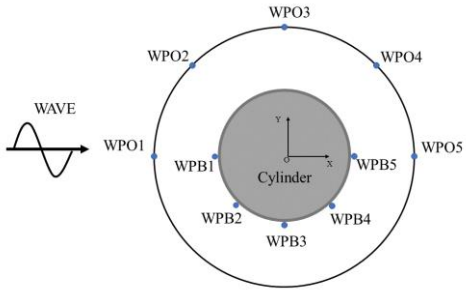

Fig. 2. Layout of wave probes

Table 1 Location of wave probes

Inner circle	*x* (m)	*y* (m)	Outer circle	*x* (m)	*y* (m)
WPB1	-8.2063	0.0000	WPO1	-16.0000	0.0000
WPB2	-5.8027	-5.8027	WPO2	-11.3137	-11.3137
WPB3	0.0000	-8.2063	WPO3	0.0000	16.0000
WPB4	5.8027	-5.8027	WPO4	11.3137	11.3137
WPB5	8.2063	0.0000	WPO5	16.0000	0.0000

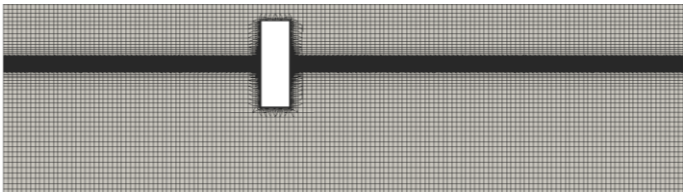

Fig. 3. Mesh of computational domain

The acquired RAOs of free surface elevations from our CFD simulation are compared with the experimental data from MOERI [13]. The RAOs of free surface elevations from potential flow solver DIFFRACT [12] are also adopted in this work. Fig. 4 shows the comparisons of the RAOs of surface elevation near the cylinder at WPB3 and WPB4 for different wave steepnesses. As shown in Fig. 4(a), for small wave steepness condition, both the CFD results and DIFFRACT results agree well with the experimental data at WPB3. As the steepness increases, the CFD solver can give more accurate prediction than the potential flow theory. This is more obvious for WPB4 in Fig. 4(b), for the *H*/*L* = 1/10 condition, the CFD solver can give a much better agreement with the experimental data. This may due to the strong nonlinear interactions at the downstream location WPB4. Reasonable agreement between the CFD results and experimental data implies that the present solver is capable to predict the wave interaction with a single cylinder.

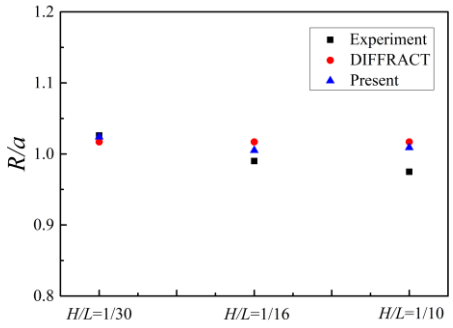

(a)WPB3

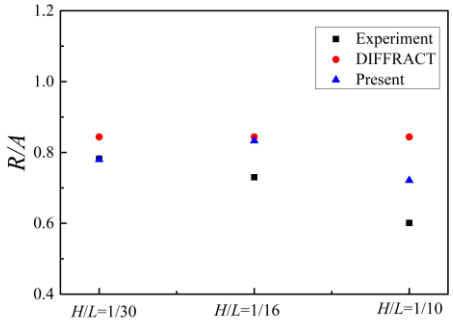

(b)WPB4

Fig. 4. Comparisons of RAOs of surface elevations

Fig. 5 shows the relative variation of the free surface elevation A/A0 (where A0 is the incident wave amplitude) at WPB1 (front), WPB3 (side) and WPB5 (behind) for different steepness parameters (*H*/*L* = 1/30, 1/16 and 1/10). The amplitudes of free surface in front of the cylinder are 1.75, 1.97 and 2.23 times than the incident wave amplitude. This indicates for higher steepness, the nonlinear interaction between wave and the cylinder is stronger.

Fig. 6 shows the time histories of horizonal wave force for three steepness parameters. The horizonal wave force increases with the wave height.

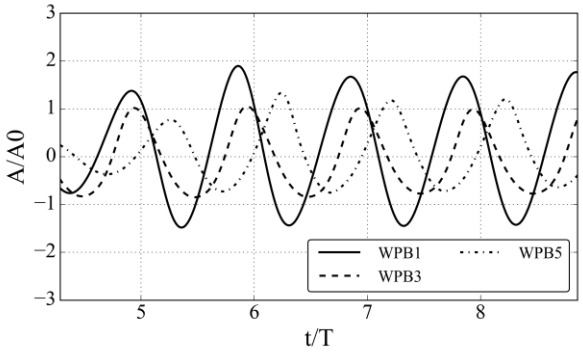

(a) *H*/*L*=1/30

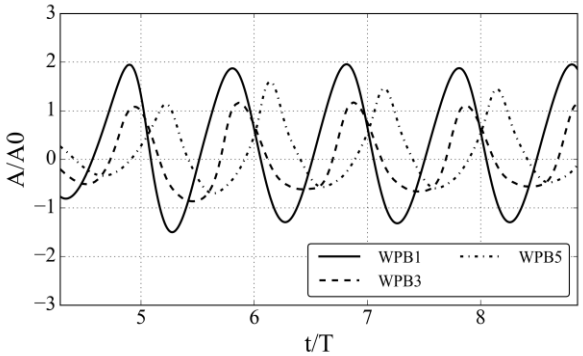

(b) *H*/*L*=1/16

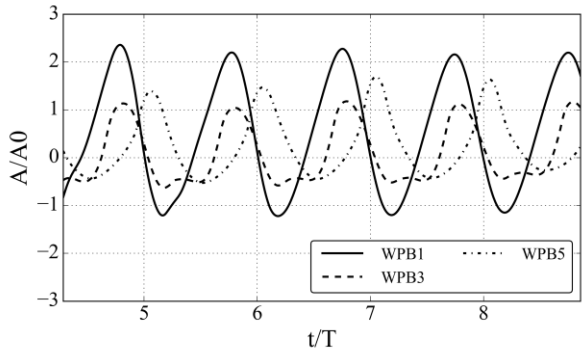

(c) H/L=1/10

Fig. 5. Free surface elevations around the cylinder for different wave steepnesses

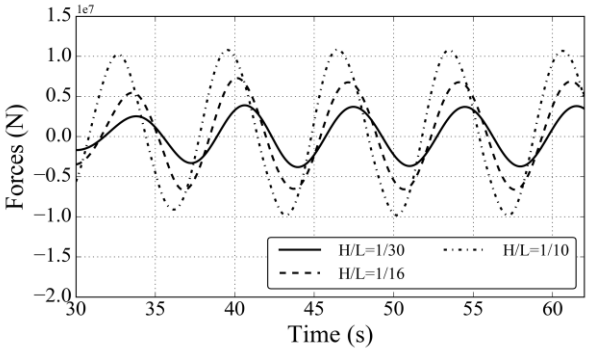

Fig. 6. Time series of horizonal wave force

Wave interaction with two tandem cylinders

To study the wave interaction with two tandem cylinders in wave propagation, numerical simulations of different center-to-center distance S are carried out. The center-to-center distance between the two cylinders are S = 34 m and 68 m. The total grid number is 2.61 million in the numerical simulation. Stokes first-order wave with wave period T = 7 s, wave height H = 7.644 m and wavelength L = 76.44 m is adopted. The upstream cylinder is marked as cylinder 1 and the downstream cylinder is cylinder 2. As we know, wave height, distance between the cylinders and wave frequency can influence the wave loads on cylinders. The effect of distance between cylinders is mainly discussed in this work.

Fig. 7 and Fig. 8 show the time histories of horizonal wave force with center-to-center distance S=34 m and 68 m, respectively. For small center-to-center distance case, the horizonal wave force of single cylinder is smaller than cylinder 1 and larger than cylinder 2. This indicates that the tandem arrangement has great influence on the wave force of cylinders and wave interaction between the cylinders is strong. For large center-to-center distance case, the wave force of cylinder 2 almost equals to that of single cylinder. The phase difference can be found for different cases.

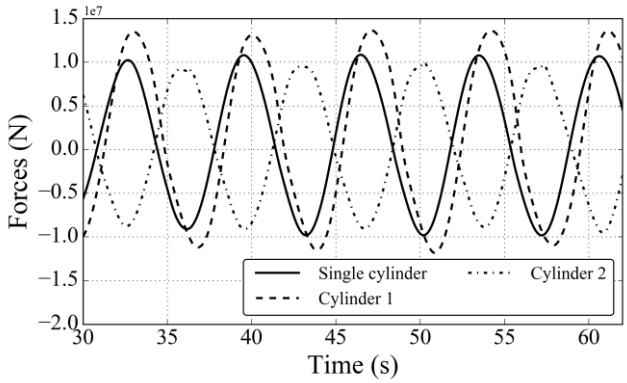

Fig. 7. Time series of horizonal wave force with center-to-center distance S=34m

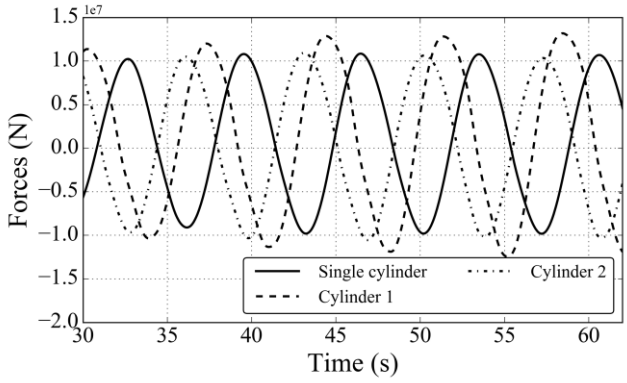

Fig. 8. Time series of horizonal wave force with center-to-center distance S=68m

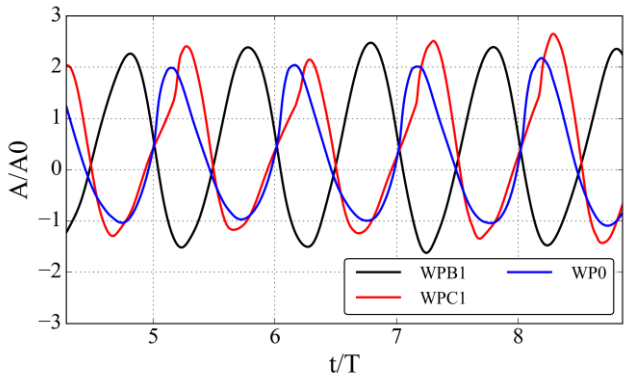

Fig. 9. Free surface elevations in front of the cylinders with center-to-center distance S=34m

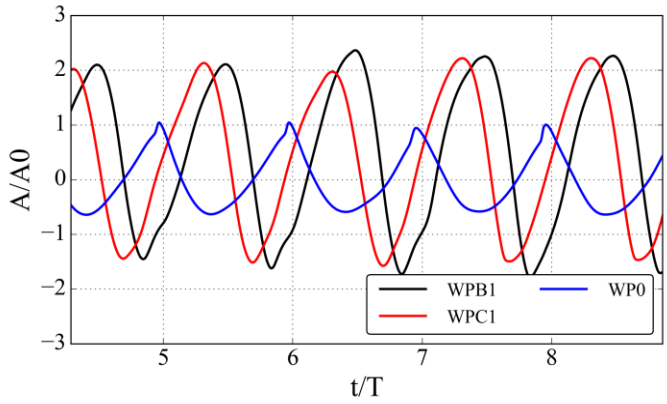

Fig. 10. Free surface elevations in front of the cylinders with center-to-center distance *S*=68m

Fig. 9 and Fig. 10 show the free surface elevations in front of the cylinders with center-to-center distance *S*=34 m and 68 m, respectively. Wave gauges are placed in front of the cylinders (WPB1 and WPC1 are in front of cylinder 1 and cylinder 2, respectively) and at the middle point between the cylinders (WP0). It is obviously seen that the crest height is increased in front of cylinder 1 and cylinder 2 in both case due to the wave run-up on the cylinders. The crest height in front of the cylinders is about 2.1 times than the incident wave amplitude. The relative crest height A/A0 in front of cylinders is similar for each case, but the waveform of cylinder 1 and cylinder 2 shows great difference for *S*=34 m and 68 m. For the larger center-to-center distance case, the waveform of cylinder1 and cylinder 2 is similar at crest and trough. For the smaller center-to-center distance case, the waveform of cylinder 1 is symmetry, while the waveform of cylinder 2 shows asymmetrical characters with shallow troughs and sharp crests. At middle point of the cylinders, the relative crest height of two cases shows great difference. The crest height for *S*=34 m case is about 2 times than the incident wave amplitude, while it almost equals to incident wave amplitude for *S*=68 m case. This indicates that when the cylinders are close to each other, the wave interaction between the cylinders can be relatively strong.

In order to investigate the wave field around the two tandem cylinders, the surface elevation in the numerical wave tank is studied. Fig. 11 and Fig. 12 show the local free surface around the tandem cylinders for *S*=34 m and 68 m. The wave diffraction patterns around the cylinders can be clearly seen for both cases. When the wave crest approaches cylinder1, the water is blocked in front of the cylinder and concentric wave field can be observed. As shown in Fig. 11(a), the surface elevation increases and the waveform changes due to the wave diffraction around cylinder 1. This is specified by Swan and Sheikh [31]. As water travels about half of cylinder 1, the free surface elevation decreases shown in Fig. 11(b) and the non-concentric wave field can be found. Fig. 11(c) shows the increase in surface elevation as the wave travels in front of cylinder 2 and two semi-circular waves can be seen. This is because the incident and reflected waves meet behind cylinder 1 and interferes with each other. Fig. 11(d) shows the decrease when wave travels over cylinder 2. Similar phenomenon can be found in Fig. 12. However, due to the larger center-to-center distance, the wave interaction between the two tandem cylinders is not so obvious.

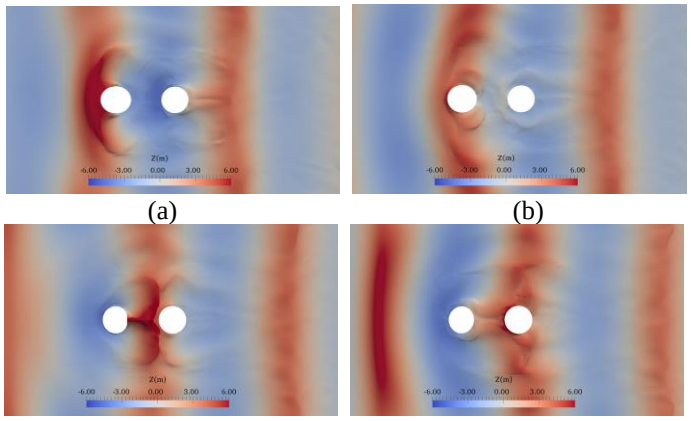

Fig. 11. Free surface elevations around the cylinders with center-to-center distance *S*=34m: (a) t/T=10, (b) t/T=10.21, (c) t/T=10.42, (d) t/T=10.86

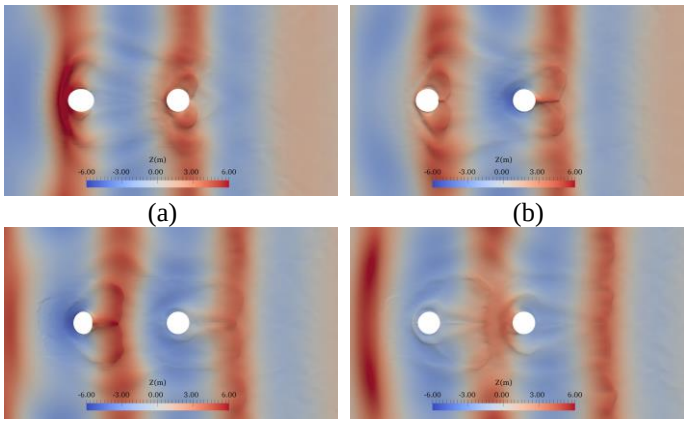

Fig. 12. Free surface elevations around the cylinders with center-to-center distance *S*=68m: (a) t/T=10, (b) t/T=10.21, (c) t/T=10.42, (d) t/T=10.86

CONCLUSIONS

In the present work, numerical simulation of regular wave interaction with a single cylinder and a pair of tandem cylinders is performed by the in-house naoe-FOAM-SJTU solver. The predicted RAOs of local surface elevation are compared with the experimental data and good agreement can be acquired even at the strong nonlinear interaction location for a single cylinder case. The amplitudes of free surface in front of the cylinder are 1.75, 1.97 and 2.23 times than the incident wave amplitude with the increasing wave steepness. For the tandem cylinders cases,

the horizonal wave force of single cylinder is smaller than cylinder 1 and larger than cylinder 2 when the center-to-center distance is small, and the waveform of cylinder 2 shows asymmetrical characters with shallow troughs and sharp crests. Different wave diffraction patterns between the cylinders can be found for different center-to-center distances. This study shows the capability of the present solver to investigate the wave run-up on a fixed cylinder. Further work should be focused on effect of wave steepnesses and wave periods on tandem cylinders.

ACKNOWLEDGMENTS

This work is supported by the National Natural Science Foundation of China (51490675, 11432009, 51579145), Chang Jiang Scholars Program (T2014099), Shanghai Excellent Academic Leaders Program (17XD1402300), Program for Professor of Special Appointment (Eastern Scholar) at Shanghai Institutions of Higher Learning (2013022), Innovative Special Project of Numerical Tank of Ministry of Industry and Information Technology of China (2016-23/09) and Lloyd's Register Foundation for doctoral student, to which the authors are most grateful.

REFERENCES

[1] Galvin, C. J., Hallermeier, R. J. Wave runup on vertical cylinders. *Coast. Eng.*, 1972, 1, 1955-1974.

[2] Chakrabarti, S. K., Tam, W. A. Wave height distribution around a vertical cylinder. *J. Waterway Div.*, 1975, 101(2), 225-230.

[3] Morris-Thomas, M. T., Thiagarajan, K., Krokstad, J. R. An experimental investigation of wave steepness and cylinder slenderness effects on wave run-up. In *Proc. 21st Int. Conf. Offshore Mech. Arctic Eng.*, Oslo, Norway, OMAE, June 23-28, 2002, OMAE2002-28050.

[4] Havelock, T. H. The pressure of water waves upon a fixed obstacle. In *Proc. R. Soc. London, Ser. A.*, 1940, 175(963), 409-421.

[5] Hunt, J. N., Baddour, R. E. The diffraction of a nonlinear progressive wave by a vertical cylinder. *Q. J. Mech. Appl. Machematics*, 1981, 34(1), 69-88.

[6] Trulsen, K., Teigen, P. Wave scattering around a vertical cylinder: fully nonlinear potential flow calculations compared with low order perturbation results and experiment. In *Proc. 21st Int. Conf. Offshore Mech. Arctic Eng.*, Oslo, Norway, June 23-28, 2002, OMAE2002-28173.

[7] Teigen, P., Niedzwecki, J. M. Wave diffraction effects and runup around multicolumn structure. In *Proc. 13th Int. Offshore Polar Eng. Conf.*, Honolulu, USA, May 25-30, 2003, 137-144.

[8] Morris-Thomas, M. T., Thiagarajan, k. The run-up on a cylinder in progressive surface gravity waves: harmonic components. *Appl. Ocean Res.*, 2004, 26(3), 98-113.

[9] Cao, H. J., Wan, D. C. Development of multidirectional nonlinear numerical wave tank by naoe-FOAM-SJTU solver. *Int. J. Ocean Syst. Eng.*, 2014, 4(1), 52-59.

[10] Cao, H. J., Wan, D. C. Benchmark computations of wave run-up on single cylinder and four cylinders by naoe-FOAM-SJTU solver. *Appl. Ocean Res.*, 2017, 65, 327-337.

[11] Cao, H. J., Wan, D. C. RANS-VOF solver for solitary wave run-up on a circular cylinder. *China Ocean Eng.*, 2015, 29(2), 183-196.

[12] Sun, L., Zang, J., Chen, L., Taylor, R. E., Taylor, P. H. Regular waves onto a truncated circular column: A comparison of experiments and simulations. *Appl. Ocean Res.*, 2016, 59, 650-662.

[13] Kristiansen, T., Baarholm, R., Stansberg, C. T. Validation of second-order analysis in predicting diffracted wave elevation around a vertical circular cylinder. In *Proc. 14th Int. Offshore Polar Eng. Conf.*, Toulon, France, May 23-28, 2004, 342-349.

[14] Niedzwecki J. M., Huston J. R. Wave interaction with tension leg platforms. *Ocean Eng.*, 1992, 19(1): 21-37.

[15] Contento G., D'Este F., Sicchiero M., Codiglia R., Calza M. Run-up and wave forces on an array of vertical circular cylinders: experimental study on second-order near trapping. *Int. J. Offshore Polar Eng.*, 2005, 15(2): 96-103.

[16] Ma Q. W., Wu G. X., Taylor R. E. Finite element simulations of fully non-linear interaction between vertical cylinders and steep waves. Part 2: numerical results and validation. *Int. J. Numer. Methods Fluids*, 2001, 36(3): 287-308.

[17] Stansberg C. T., Kristiansen T. Non-linear scattering of steep surface waves around vertical columns. *Appl. Ocean Res.*, 2005, 27(2): 65-80.

[18] Ohl C. G., Taylor R. E., Taylor P. H., Borthwick A. L. Water wave diffraction by a cylinder array. Part 1. Regular waves. *J. Fluid Mech.*, 2001, 442, 1-32.

[19] Ohl C. G., Taylor P. H., Taylor R. E., Borthwick A. L. Water wave diffraction by a cylinder array. Part 2. Irregular waves. *J. Fluid Mech.*, 2001, 442, 33-66.

[20] Ji X., Li J., Liu S., Zhang H. Real Sea Waves Interaction with an Array of Cylinders in Tandem. In *Proc. 27th Int. Offshore Polar Eng. Conf.*, San Francisco, USA, June 20-25, 2017, 1411-1414.

[21] Kamath A., Chella M. A., Bihs. H. CFD investigations of wave interaction with a pair of large tandem cylinders. *Ocean Eng.*, 2015, 108: 738-748.

[22] Zhong Q, Yeung R. W. Wave-body interactions among an array of truncated vertical cylinders. In *Proc. 35th Int. Conf. Offshore Mech. Arctic Eng.*, Busan, South Korea, June 19-24, 2016, OMAE2016-55055.

[23] Shen, Z. R., Wan, D. C., Carrica, P. M. Dynamic overset grids in OpenFOAM with application to KCS self-propulsion and maneuvering. *Ocean Eng.*, 2015, 108, 287-306.

[24] Shen, Z. R., Wan, D. C. An irregular wave generating approach based on naoe-FOAM-SJTU solver. *China Ocean Eng.*, 2016, 30(2), 177-192.

[25] Wang, J. H., Wan, D. C. Numerical simulation of pure yaw motion using dynamic overset grid technology. *Chinese J. Hydrodyn.*, 2016, 31, 567-574.

[26] Ye, H. X., Wan, D. C. Benchmark computations for flows around a stationary cylinder with high Reynolds numbers by RANS-overset grid approach. *Appl. Ocean Res.*, 2017, 65, 315-326.

[27] Liu, Z. H., Wan, D. C. Numerical simulation of green water on S-175 containership. In *Proc. Second Conf. Global Chinese Scholars Hydrodyn.*, Wuxi, China, November 11-14, 2016, 815-821.

[28] Hirt, C. W., Nichols, B. D. Volume of fluid (VOF) method for the dynamics of free boundaries. *J. Comput. Phys.*, 1981, 39(1), 201-225.

[29] Hajivand, A., Mousavizadegan, S. H. Virtual maneuvering test in CFD media in presence of free surface. *Int. J. Nav. Arch. Ocean Eng*., 2015, 7(3), 540-558.

[30] Stern, F., Wilson, R., Shao, J. Quantitative V&V of CFD simulations and certification of CFD codes. *Int. J. Numer Meth. FL.*, 2006, 50(11), 1335-1355.

[31] Swan, C., Sheikh, R. The interaction between steep waves and a surface-piercing column. *Philos. Trans. R. Soc. London, Ser. A.*, 2015, 373(2033), 20140114.